JOURNAL OF GUIDANCE, CONTROL, AND DYNAMICS
Vol. 20, No. 5, September–October 1997

Robust Longitudinal Control Design Using Dynamic Inversion and Quantitative Feedback Theory

S. Antony Snell* and Perry W. Stout†
University of California, Davis, Davis, California 95616

The objective is to design low-bandwidth control laws that yield robust performance over a wide flight envelope in the presence of 20% model uncertainties. This is achieved by using a hybrid controller in which a second-order dynamic inversion transforms the nonlinear angle-of-attack dynamics to linear time-invariant form, while an outer loop, designed using quantitative feedback theory (QFT), ensures robust performance. The dynamic inversion reduces the plant variations due to nonlinearity, which are traditionally treated as uncertainty in QFT. The reduced uncertainty allows lower controller bandwidth for a given level of performance. The hybrid controller design is applied to the unstable, nonlinear, short-period dynamics of the F-16 aircraft and compared with a baseline QFT controller designed without dynamic inversion. Both designs provide satisfactory performance, but the baseline QFT controller requires a bandwidth of around 4–8 rad/s, whereas the hybrid design has a bandwidth of only about 1 rad/s, leading to reduced demands on the control hardware. The success of the dynamic inversion depends strongly on the desired linear dynamics, and so recommendations are given on their selection.

Nomenclature

$C_{m_{\text{total}}}$	= nondimensional pitch moment coefficient
$C_{m_\alpha}, C_{m_q}, C_{m_{\delta_e}}$	= nondimensional partial derivative of $C_{m_{\text{total}}}$ with respect to α, q, and δ_e
$C_{X_{\text{total}}}, C_{Z_{\text{total}}}$	= nondimensional coefficient of x/z force
$\bar{c}$	= mean aerodynamic chord
I_{yy}	= moment of inertia about pitch axis
M	= aerodynamic pitch moment, $M = \bar{q}S\bar{c}C_{m_{\text{total}}}$
m	= mass
q	= pitch rate, $\dot{\theta}$
$\bar{q}$	= dynamic pressure, $\frac{1}{2}\rho V^2$
S	= swept area of wings
u, w	= body x and z components of velocity
V	= magnitude of velocity
X	= aerodynamic force in body x, $\bar{q}SC_{X_{\text{total}}}$
Z	= aerodynamic force in body z, $\bar{q}SC_{Z_{\text{total}}}$
α	= angle of attack, $\tan^{-1}(w/u)$
δ_e	= elevator deflection
θ	= pitch attitude angle

I. Introduction

ALTHOUGH it is unconventional, poststall flight provides aircraft with a decisive advantage during close-in combat over similar aircraft without such capabilities.[1] Designing control laws for poststall flight is challenging because the prevailing dynamics are uncertain and contain nonlinearities arising from both aerodynamics and inertial coupling terms. Figure 1 shows that C_m for the F-16 is a highly nonlinear function of angle of attack (AOA) and δ_e when AOA exceeds 35 deg. This paper presents a method for designing control laws for flight over a wide envelope including poststall flight.

One approach to flight control is to design a single, linear controller with sufficient robustness to provide good performance in the presence of large variations in aircraft dynamics. Powerful tools exist to design robust, linear control laws, notably μ-synthesis and quantitative feedback theory (QFT). There is a rigorous mathematical background for μ-synthesis, but it still relies on the designer to select appropriate penalty weightings and it yields controllers of undesirably high order.[2] In contrast, QFT[3–6] provides a fairly direct path to robust control design for the single-input/single-output (SISO) case. QFT has a history of flight control applications; for example, Hess and Gorder[7] use QFT to design a multi-input/multi-output (MIMO) control law for wide envelope helicopter flight, whereas Reynolds et al.[8] apply QFT to a highly maneuverable combat aircraft.

In the present study, a fixed-gain linear controller was constructed as a baseline for comparison purposes. It was designed using an extension of QFT to nonlinear systems[4] in which a set of linear time-invariant equivalent (LTIE) models substitutes for the nonlinear aircraft dynamics. One of the shortcomings of using a fixed-gain controller is that it must be robust to large variations in aircraft dynamics over the whole envelope. This often requires high loop gain, which can lead to poor performance in the presence of unmodeled dynamics and sensor noise. To address this problem, Horowitz[9] proposes a nonlinear cancellation scheme to precondition the nonlinear dynamics into a linear form before applying QFT, which permits considerable loop gain reduction. This is similar to the hybrid designs in this paper. The authors' first attempt to address this issue[10] used a single gain proportional to $1/V$, which was placed in series with the QFT compensator to offset the gain variation caused by the dependence of elevator effectiveness on V^2. This reduces the size of some uncertainty templates, permitting lower gain to be used at high speed. However, the improvements were limited because, although the high-frequency templates shrink, lower-frequency templates grow. This was explained by examining the linearized dynamics between δ_e and α (Ref. 10).

The conventional approach to control law synthesis for flight over a wide envelope is to schedule the linear controller gains as functions of slowly varying parameters such as V. Gain scheduling with respect to a more rapidly changing variable such as α can lead to stability problems.[11] Furthermore, designing the schedules is usually laborious and time consuming.

Dynamic inversion provides a systematic alternative to gain scheduling.[12–14] The multiple linearized models required for gain scheduling are not needed because dynamic inversion applies directly to the nonlinear dynamic equations. The procedure is to rearrange the equations to compute the control inputs required to cancel the nonlinear terms and replace them with desirable linear terms. The choice of desired dynamics is critical to the success of this method. It is also important that the mathematical model is an accurate representation of the real aircraft, which is often not the case in practice. Reference 14 suggests that dynamic inversion can perform

Presented as Paper 96-3783 at the AIAA Guidance, Navigation, and Control Conference, San Diego, CA, July 29–31, 1996; received Sept. 13, 1996; revision received April 29, 1997; accepted for publication May 12, 1997.

*Assistant Professor, Mechanical and Aeronautical Engineering. Senior Member AIAA.

†Graduate Student, Mechanical and Aeronautical Engineering. Senior Member AIAA.

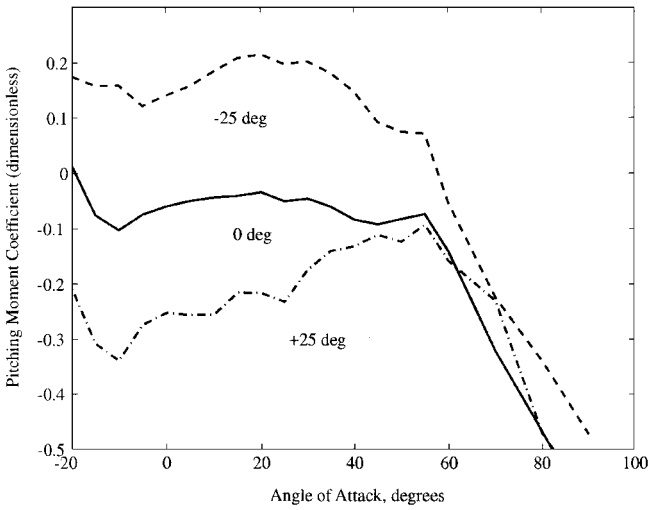

Fig. 1 F-16 pitching moment coefficient C_m as a function of α and δ_e.

well in the presence of perturbations to the dynamics. However, this robustness is often achieved by using high gains.

In this paper, low-bandwidth inner loops using dynamic inversion are constructed to cancel the nonlinearities in the aircraft dynamics and then QFT is applied to design an outer loop, which endows the closed loop with robust performance. The two methods complement one another: dynamic inversion reduces the size of the uncertainty templates used in the QFT process because the plant variations due to nonlinearity are conventionally treated as uncertainty. Reduced template size allows reduced controller bandwidth for a given level of performance. Meanwhile, the dynamic inversion can use lower bandwidths because robustness to uncertainties is ensured by the QFT design rather than by simply increasing the dynamic inversion gains. References 15 and 16 describe a related technique in which dynamic inversion is combined with μ-synthesis.

An earlier paper used a first-order, dynamic inversion to linearize the pitch rate q dynamics only and then used QFT to design an outer loop to control AOA.[17] The dynamic inversion inner loop used a gain on q of only 3 rad/s, which is lower than conventional dynamic inversion,[12–14] because the QFT provided robustness to model uncertainty. Although a first-order inversion such as this was easy to design and implement, it did not completely linearize the AOA dynamics. Nonlinear terms due to lift force remained in the $\dot{\alpha}$ equation, and so the dynamics varied with changes in V and α. Despite this, there was sufficient reduction in template size to realize a worthwhile reduction in gain compared to the baseline linear QFT design.

In the current study, a second-order inversion of the α dynamics is combined with an outer QFT loop with the objective of lowering bandwidth further. The second-order dynamic inversion almost exactly linearizes the dynamics between the pseudoinput ν and the output α. This eliminates variation in the plant dynamics caused by nonlinearities in the equations of motion, which reduces the size of the QFT templates.

The remainder of this paper is as follows. First, QFT and dynamic inversion are briefly introduced. Then the simplified short-period model used to conduct simulations is presented. Specific details of the control law designs follow. Finally, simulations are discussed and conclusions are presented.

II. QFT

Further discussion of QFT may be found in Refs. 3–6. QFT was originated by Horowitz[3] and has been successfully applied to highly uncertain, linear time-invariant, SISO plants. There are extensions of the idea to MIMO, nonlinear, and time-varying plants.[4–8] The objective of QFT is to select a feedback compensator $G(s)$ and prefilter $F(s)$ (Fig. 2) to ensure that the output response to a given input falls within the set of acceptable time responses $\mathcal{A}$ for any plant in the set of possible plants $\mathcal{P}$. This is achieved by putting specifications on $T_{yr}(s)$, the closed-loop transfer function between r and y.

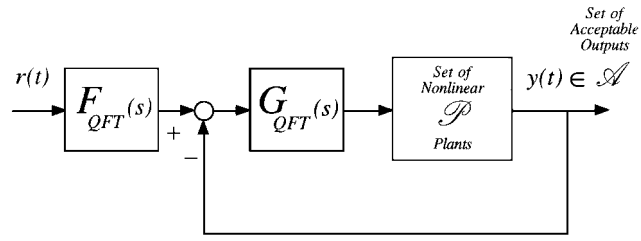

Fig. 2 Two-DOF nonlinear QFT control configuration.

From Fig. 2, it is seen that $T_{yr}(s) = T(s)F(s)$, where

$$T(s) = \frac{P(s)G(s)}{1 + P(s)G(s)} \tag{1}$$

First, $G(s)$ is selected to ensure that $T(s)$ is insensitive enough to the possible variations in $P(s)$ so that $T_{yr}(s)$ does not vary by more than is allowed by the specification at each frequency. High gain in $G(s)$ such that $PG(j\omega) \gg 1$ at a given frequency causes $T(j\omega)$ to be close to unity regardless of perturbations in $P(s)$. $G(s)$ is usually designed on the Nichols chart. At each selected frequency, a connected region or template P is constructed, enclosing all of the individual points produced by the plants included in $\mathcal{P}$. The larger the template, the more uncertain is the plant at that frequency. The Nichols chart is convenient because the M curves are contours of constant magnitude of $T(j\omega)$ and also because multiplying all of the elements in the template P by $G(j\omega)$ simply translates P on the chart; the size, shape, and orientation of P do not change. An ideal $G(s)$ provides just enough gain to place a template between two M curves corresponding to an acceptable magnitude variation and no further. Finally, $F(s)$ is designed using Bode magnitude plots of $T(s)$ to ensure that $T_{yr}(s)$ meets its frequency response specifications.

When QFT is applied to nonlinear plants, the technique is extended[4] by using LTIE systems, which most closely reproduce the response of the nonlinear system to given inputs. LTIE models of the aircraft are extracted using GOLUBEV, an algorithm implemented in MATLAB due to Golubev and Horowitz.[18] GOLUBEV takes the time histories of input and output signal pairs and numerically determines a transfer function relating the two. Thus, a LTIE model is not simply a linearization of the model about an equilibrium point, which is often only valid close to equilibrium. Instead, a LTIE model may substitute for the dynamics in a much larger region. Inasmuch as the aircraft is a nonlinear system, a whole set of LTIE models is required to accurately reproduce the nonlinear response to arbitrary input signals. This set serves to define the set $\mathcal{P}$, from which templates P are constructed. Then QFT is used to design a controller, which produces acceptable responses for the whole set of LTIE models. Schauder's fixed-point theorem[4] guarantees that the response of the nonlinear system will also be acceptable, as long as the LTIE model, which characterizes the nonlinear aircraft response in a given maneuver, is included in $\mathcal{P}$. The compensator resulting from this design approach tends to be conservative because an accurately determined nonlinearity may yield a widely scattered set of LTIE models. The full extent of $\mathcal{P}$ depends on the spread of the LTIE models. The number of models to include is not clear-cut but should include models corresponding to the most extreme maneuvers at the most extreme parts of the operating envelope together with a cross section of points closer to nominal conditions. The number of combinations can increase rapidly when there are several independent model parameters to consider, so judgment must be exercised to limit the number of model extractions needed to realistically characterize $\mathcal{P}$. For example, when the perturbed aerodynamic data are used, three derivatives may be perturbed up 20%, nominal, or down 20%. This yields 27 possibilities for each simulation run. However, in perturbed simulations, only the extremes were chosen so that a derivative was either +20 or −20% because it is the extreme values that will have the largest effect on the responses. Furthermore, rather than perturbing the data for every simulation, only the simulations on the limits of the templates with nominal data were rerun with perturbed data.

III. Nonlinear Dynamic Inversion

Dynamic inversion is a systematic method for designing control laws for nonlinear systems and has been proposed for flight control.[12–14] The basic idea is to solve for the control input required in the dynamic equations to give a specific output. It relies on knowledge of the nonlinear dynamic equations alone rather than linearizations about various operating points.

For example, consider the first-order nonlinear pitch dynamics

$$\dot{q} = f(q, \alpha, V, \delta_e) \tag{2}$$

Equation (2) is rearranged to solve for the δ_e, which yields the desired $\dot{q}_{\text{des}}$ exactly,

$$\delta_e = f^{-1}(\dot{q}_{\text{des}}, q, \alpha, V) \tag{3}$$

This example is a first-order inversion, where the control input δ_e acts directly on the first derivative of q. The state, α, is not controlled directly using a first-order inversion because the elevator has only a small effect on $\dot{\alpha}$ caused by the small direct lift force it generates. Direct lift control would require much larger elevator surfaces. In conventional aircraft, such as the F-16, the elevator is configured to produce large pitching moments to generate $\dot{q}$ directly. Therefore, a first-order inversion may be used to compute the δ_e necessary to produce $\dot{q}_{\text{des}}$, whereas a second, first-order inversion is used to compute the commanded pitch rate q that yields the desired $\dot{\alpha}$. This approach is referred to as multiple time scaling and has been shown to work well,[12–14,16,17] although it requires some approximations.

In the present study, the authors construct a second-order, dynamic inversion control law, which uses the elevator input δ_e to directly control the second derivative $\ddot{\alpha}$. This is reasonable to do because δ_e has a significant effect on $\ddot{\alpha}$ even though its effect on $\dot{\alpha}$ is small. This eliminates the need to control q directly and also promises more accurate control of AOA itself.

IV. F-16 Model

Nguyen et al.[19] give data for a six-degree-of-freedom (DOF), nonlinear, rigid-body model of the F-16 aircraft, including tabular aerodynamic data of force and moment coefficients for AOA from −20 to +90 deg. The model used here is a short-period model derived from those data with V set to a constant value in any given maneuver, as discussed in Ref. 10:

$$\dot{\alpha} = q + \frac{mg\cos\theta + Z}{mV\cos\alpha} \tag{4a}$$

$$\dot{q} = M/I_{yy} \tag{4b}$$

$$\dot{\theta} = q \tag{4c}$$

An algebraic expression for the thrust T is also obtained:

$$T = -X + Z\tan\alpha + mg(\sin\theta - \tan\alpha\cos\theta) \tag{5}$$

Equations (4a–4c) and (5) constitute the short-period model. The three states, α, q, and θ, are augmented by elevator dynamics, modeled as a first-order lag with a time constant of 0.050 s. The elevator deflection[19] is limited to ±25 deg with a slew rate limit of 60 deg/s. The aerodynamic data are provided in the following form:

$$C_{X_{\text{total}}} = C_X(\alpha, \delta_e) + C_{X_q}(\alpha)q(\bar{c}/2V) \tag{6a}$$

$$C_{Z_{\text{total}}} = C_Z(\alpha, \delta_e) + C_{Z_q}(\alpha)q(\bar{c}/2V) \tag{6b}$$

$$C_{m_{\text{total}}} = C_m(\alpha, \delta_e) + C_{m_q}(\alpha)q(\bar{c}/2V) \tag{6c}$$

where C_X, C_Z, and C_m are tabulated at 5-deg intervals in α and for δ_e equal to −25, −10, 0, 10, and 25 deg. These grid points are sufficiently close so that linear interpolation can be used. Custom-built, two-dimensional, table-lookup functions parameterized by α and δ_e were constructed to use these data directly. The entire model was implemented using MATLAB.

V. Design Specifications

The objective of the flight control law is to allow the pilot to control AOA accurately during high-AOA maneuvers. The design specifications are given in terms of time-domain responses to test signals involving various step changes in $\alpha_{\text{stick}}(t)$. The set of acceptable responses $\mathcal{A}$ is shown in Fig. 3 and includes first-order and moderately damped, second-order responses with less than 20% overshoot. These responses are interpreted as bounds on the frequency response of $T_{yr}(s)$, the closed-loop transfer function between $\alpha_{\text{stick}}(t)$ and $\alpha(t)$ (Fig. 4).

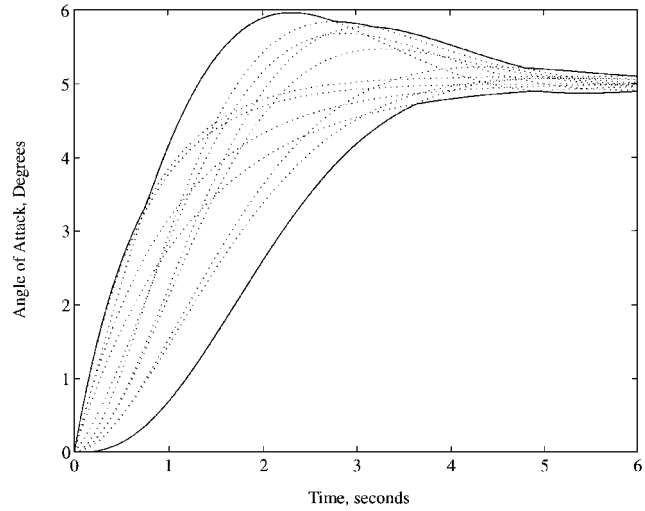

Fig. 3 Set of acceptable time-domain responses to a 5-deg α step.

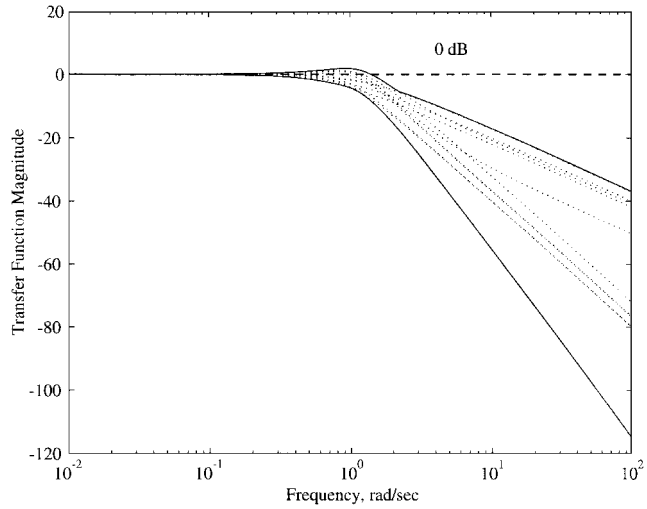

Fig. 4 Equivalent acceptable closed-loop frequency responses.

The difference between the upper and lower bounds in Fig. 4 yields a specification on the maximum allowable magnitude variations of $T_{yr}(s)$: 0.32, 0.76, 2.47, 5.99, 11.1, 22.3, and 34.4 dB at the frequencies $\frac{1}{8}$, $\frac{1}{4}$, $\frac{1}{2}$, 1, 2, 4, and 8 rad/s, respectively.

VI. Baseline QFT Design

The short-period F-16 model is unstable, and so it was stabilized using an inner q loop before conducting the QFT design. The selection of the feedback gain $K_q = -40$ deg/(rad/s) is described in Ref. 10. This q loop remained part of the baseline flight control law shown in Fig. 5.

A. LTIE Models

LTIE models were obtained by using GOLUBEV to fit transfer functions between matched pairs of $\alpha(t)$ output and $u(t)$ input signals. The signal pairs must be such that $\alpha(t)$ is within the bounds of $\mathcal{A}$ (Fig. 3). The method used to generate these signal pairs for the baseline QFT controller was to substitute a high-gain controller $G_{\text{HG}}(s)$ in place of $G_{\text{QFT}}(s)$ and setting $F_{\text{HG}}(s) = T_{\text{des}}(s)$ in Fig. 5. An acceptable $T_{\text{des}}(s)$ meeting the magnitude specifications of Fig. 4 causes the loop input, $\alpha_{\text{filt}}(t) \in \mathcal{A}$. The high loop gain forces the actual $\alpha(t)$ to track $\alpha_{\text{filt}}(t)$ so closely that it also falls within $\mathcal{A}$. The input signal to the q loop, $u(t)$, which is generated within the high-gain α loop, is then paired with the acceptable output signal $\alpha(t)$.

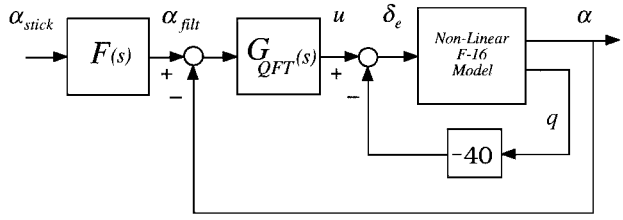

Fig. 5 Baseline α control configuration with inner q loop.

The high-gain α loop is implemented merely to get input/output signal pairs and has nothing to do with the final flight control law. $G_{\mathrm{HG}}(s)$ is deliberately designed to give a high crossover frequency (>10 rad/s) so that the $\alpha(t)$ signal closely follows $\alpha_{\mathrm{filt}}(t)$. Because the relationship between $u(t)$ and $\alpha(t)$ is nonminimum phase, the high-gain controller must be designed with care. Sometimes a different high-gain controller must be designed for each flight condition, but here two different high-gain controllers sufficed. The first was effective for speeds from 78 to 150 m/s:

$$G_{\mathrm{HG}_1}(s) = \frac{-2481(s+1)(s+10)}{s(s+50)} \tag{7a}$$

The second was used for the low-speed simulations at 53 and 62 m/s:

$$G_{\mathrm{HG}_2}(s) = \frac{-8000(s+1)^2}{s(s+50)} \tag{7b}$$

With the high-gain controllers implemented, 44 simulations of pull-up and push-over maneuvers of varying severity were conducted at the speeds 53, 62, 78, 97, 120, and 150 m/s to provide reasonable coverage of the flight envelope. Nominal aerodynamic data were used in each of these simulations. Uncertainty templates were formed with nominal data, as will be described. Then eight additional high-gain simulations were run for each of nine specific flight conditions with the derivatives C_{m_α}, $C_{m_{\delta_e}}$, and C_{m_q} perturbed by ±20% to yield an additional 72 LTIE models. The nine flight conditions selected for the perturbed simulations were chosen because their nominal LTIE models had formed vertices of the nominal templates.

B. Templates and QFT Design

The magnitudes and phases of all 116 LTIE transfer functions were plotted on the Nichols chart at the design frequencies of interest: $\frac{1}{8}$, $\frac{1}{4}$, $\frac{1}{2}$, 1, 2, 4, and 8 rad/s. These frequencies represent the primary open-loop design region three octaves above and three octaves below the desired, closed-loop bandwidth. Templates were constructed as shown in Fig. 6, and one of the LTIE models was selected as the nominal plant to provide the templates with handles.

Designing $G(s)$ is straightforward. $G(s)$ must move the handle transfer function on the Nichols chart so that at each design frequency the handle lies on or above the tracking boundary curves and outside the overshoot M circle for that frequency. The tracking boundaries were computed by sweeping the templates across the Nichols chart from 0 to −200 deg in 5-deg steps while moving them high enough vertically until they fit between a pair of M curves with the same closed-loop magnitude variation as allowed by the specifications on $T_{yr}(s)$ discussed in Sec. V. The loci of points swept out by the template handles as they traverse the Nichols chart form the tracking bounds. A second, stability bound is the maximum allowable overshoot boundary or M circle limit. This curve is formed by translating the templates around the specified M circle while tracing the locus of handle points.

The selected compensator is

$$G_{\mathrm{QFT}}(s) = \frac{-41{,}800[s^2 + 1.2(0.38)s + 0.38^2](s+2.1)}{s(s+0.05)[s^2 + 1.4(20)s + 20^2]} \tag{8}$$

The source of the minus sign in Eq. (8) is the sign convention on elevator deflection.

Figure 7 shows the effects of this compensator on the handle transfer function and the templates. Most but not all of the performance specifications were satisfied. The templates at $\frac{1}{8}$ and $\frac{1}{4}$ rad/s

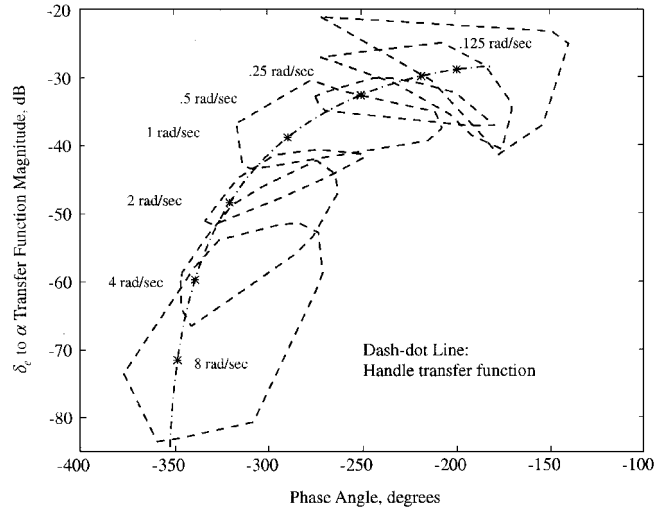

Fig. 6 Baseline QFT uncertainty templates $P(j\omega)$.

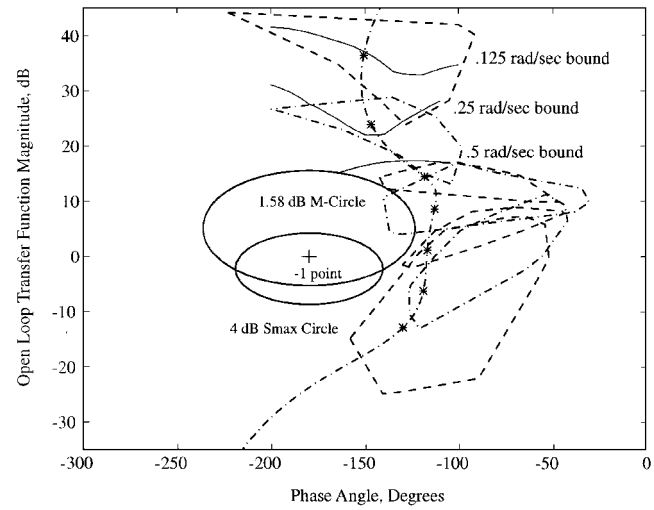

Fig. 7 Compensated baseline templates $PG(j\omega)$.

both meet their tracking bounds, which should give good, steady-state command following. However, the $\frac{1}{2}$-rad/s template handle lies slightly below its tracking bound, which may lead to slower than expected settling times at some flight conditions. The higher-frequency templates are not constrained by tracking bounds. It is also seen that all except the 1-rad/s template remain outside the 1.58-dB (20% overshoot) M circle. The small boundary violation by the 1-rad/s template was a worthwhile sacrifice because it permits much lower loop gain to be used, although it may lead to increased overshoot for a few flight conditions.

Figure 7 shows that the templates cross over between 2 and 8 rad/s for most flight conditions. Because the desired closed-loop bandwidth of $T_{yr}(s)$ is about 1 rad/s, prefiltering is required. The selected prefilter is

$$F_{\mathrm{QFT}}(s) = \frac{(1.15)^2}{s^2 + 1.4(1.15)s + (1.15)^2} \tag{9}$$

VII. Hybrid QFT Dynamic Inversion Control Law Design

The hybrid design follows a procedure similar to the baseline QFT design but, first, inner loops incorporating dynamic inversion are constructed to linearize the AOA dynamics (as shown in Fig. 8). Then a set of LTIE models is extracted from high-gain simulations with the dynamic inversion control implemented. The LTIE models represent the dynamics between output $\alpha(t)$ and the pseudoinput $\nu(t)$. After forming uncertainty templates from these new LTIE models, $G(s)$ and $F(s)$ are designed as for the baseline in Sec. VI.B.

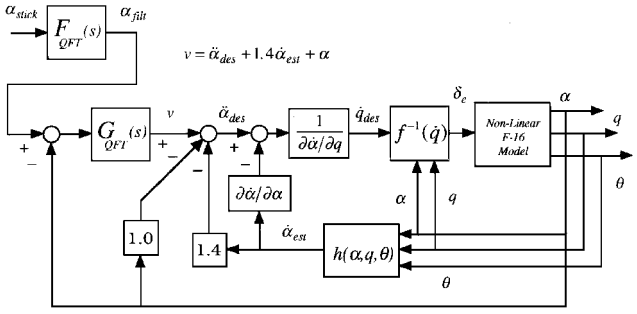

Fig. 8 Hybrid QFT plus dynamic inversion with $\ddot{\alpha}_{des} = \nu - \alpha - 1.4\dot{\alpha}_{est}$.

A. Desired Dynamics

Dynamic inversion enforces a desired linear relationship between the pseudoinput $\nu(t)$ and the output $\alpha(t)$. This is represented by the transfer function $P_{DI}(s) = \hat{\alpha}(s)/\hat{\nu}(s)$, where the carets denote Laplace transforms of $\alpha(t)$ and $\nu(t)$. The choice of $P_{DI}(s)$ is critical to the success of this method. In pure dynamic inversion designs,[12–14] $P_{DI}(s)$ is usually selected as the final closed-loop transfer function, which provides the nominal performance (Sec. V). However, this choice may not produce satisfactory performance when the plant is perturbed from nominal. Conversely, it may turn out that this choice of $P_{DI}(s)$ yields a higher bandwidth than is necessary to provide robustness to the actual level of plant uncertainties that may be present.

In this hybrid, QFT dynamic inversion design, $P_{DI}(s)$ is selected to have just enough bandwidth to ensure that variations in the magnitude of $P_{DI}(s)$ are smaller than the perturbations of the plant due to uncertainty. The performance robustness in the presence of the remaining perturbations in $P_{DI}(s)$ is ensured by using the compensator $G(s)$, and then the final closed-loop transfer function is shaped by prefilter $F(s)$, the usual two-DOF QFT approach.

The design of most aircraft is such that the natural dynamics between δ_e and $\ddot{\alpha}$ are second order. To ensure a realizable dynamic inversion, $P_{DI}(s)$ should also be at least second order. The actuator deflection δ_e is composed of both ν and state feedback through the dynamic inversion, and so it is important to limit the bandwidth of the dynamic inversion. One idea might be to select $P_{DI}(s) = 1/s^2$. The rationale is that the open-loop aircraft is unstable and so putting the poles at $s = 0$ would require least effort. As will be seen, this choice of $P_{DI}(s)$ is especially bad. The dynamic inversion can never be exact, and so the perturbed dynamics end up being $P_{DI}(s) = (1 + \varepsilon_1)/(s + \varepsilon_2)(s + \varepsilon_3)$, where the ε are caused by uncertainties in the state equations. Small variations in the locations of the poles of the open-loop plant at any fixed flight condition lead to large variations in the magnitude of $P_{DI}(s)$ at low frequency where $|s|$ is small. This leads to a lot of scatter on the Nichols chart in the presence of even these small perturbations. Furthermore, the benefits of the two integrators in $P_{DI}(s)$ for zero steady-state errors cannot be relied upon because the ε shift the poles away from $s = 0$.

A basic rule of thumb is to select $P_{DI}(s)$ with stable poles having the same magnitude as the poles of linearizations of the open-loop aircraft. Consider the following linearization:

$$\dot{\alpha} = (Z_\alpha/V)\alpha + [1 + (Z_q/V)]\,q + \left(Z_{\delta_e}/V\right)\delta_e \qquad (10a)$$

$$\dot{q} = M_\alpha\alpha + M_q q + M_{\delta_e}\delta_e \qquad (10b)$$

where

$$Z_\alpha = \frac{\bar{q}SC_{Z_\alpha}}{m}, \qquad Z_q = \frac{\bar{q}S\bar{c}C_{Z_q}}{2mV}, \qquad Z_{\delta_e} = \frac{\bar{q}SC_{Z_{\delta_e}}}{m}$$

and

$$M_\alpha = \frac{\bar{q}S\bar{c}C_{m_\alpha}}{I_{yy}}, \qquad M_q = \frac{\bar{q}S\bar{c}^2C_{m_q}}{2VI_{yy}}, \qquad M_{\delta_e} = \frac{\bar{q}S\bar{c}C_{m_{\delta_e}}}{I_{yy}}$$

This system has a characteristic equation,

$$s^2 - [(Z_\alpha/V) + M_q]s + (Z_\alpha/V)M_q - [1 + (Z_q/V)]\,M_\alpha = 0 \qquad (11)$$

Suppose M_α, M_q, Z_α, and Z_q can vary by $\pm 20\%$ at any given flight condition; then the poles can vary by approximately $\pm 20\%$. If the poles of $P_{DI}(s)$ are chosen much smaller than those of the plant, the variation will be proportionally much larger. By studying the data in Ref. 19, the following estimates were made: $C_{m_\alpha} = 0.573$, $C_{m_q} = -6$, $C_{Z_\alpha} = -4.58$, and $C_{Z_q} = 0$. Combining these with the data $m = 9295$ kg, $I_{yy} = 75{,}674$ kg·m^2, $\bar{c} = 3.45$ m, and $S = 27.87$ m^2 yields poles at $s = -5.04$ and $+1.38$ for $V = 150$ m/s. These poles scale in direct proportion to V so that for $V = 50$ m/s the poles are at $s = -1.68$ and $+0.46$. If $P_{DI}(s)$ has stable poles of similar magnitude to the open-loop poles, then the sensitivity of the poles to perturbations in the dynamics is about the same as the open loop. Furthermore, such a choice has the important benefit of approximating an optimal control in which the control energy is minimized. Thus, the final choice for $P_{DI}(s)$ was

$$P_{DI}(s) = \frac{\hat{\alpha}(s)}{\hat{\nu}(s)} = \frac{1}{s^2 + 1.4s + 1} \qquad (12)$$

These dynamics actually satisfy the nominal closed-loop tracking specification on their own without a QFT loop. Rearranging Eq. (12) yields the desired $\ddot{\alpha}_{des}$,

$$\ddot{\alpha}_{des} = \nu - 1.4\,\dot{\alpha} - \alpha \qquad (13)$$

B. Second-Order Dynamic Inversion

The dynamic inversion is carried out by solving the dynamic equations to find the elevator deflection δ_e required to generate $\ddot{\alpha}_{des}$. This is accomplished in two steps. First, the required pitch acceleration $\dot{q}_{des}$ is found; then, δ_e is determined.

Differentiating Eq. (4a) yields an expression for $\ddot{\alpha}$,

$$\ddot{\alpha} = \frac{\partial\dot{\alpha}}{\partial\alpha}\dot{\alpha} + \frac{\partial\dot{\alpha}}{\partial q}\dot{q} + \frac{\partial\dot{\alpha}}{\partial\delta_e}\dot{\delta}_e \qquad (14)$$

The effect of δ_e on $\dot{\alpha}$ is small, and so the third term in Eq. (14) is neglected in the dynamic inversion. However, the effect of $\dot{q}$ predominates, and so Eq. (14) is rearranged to determine the $\dot{q}$ necessary to give $\ddot{\alpha} = \ddot{\alpha}_{des}$:

$$\dot{q}_{des} = \frac{1}{\partial\dot{\alpha}/\partial q}\left(\ddot{\alpha}_{des} - \frac{\partial\dot{\alpha}}{\partial\alpha}\dot{\alpha}\right) \qquad (15)$$

Thus, if $\dot{q} = \dot{q}_{des}$, then $\ddot{\alpha} = \ddot{\alpha}_{des} + \varepsilon(t)$, where $\varepsilon(t)$ is the small error introduced by neglecting the $\dot{\delta}_e$ term from Eq. (14), and the control law can be made robust to such errors. The δ_e, which ensures that $\dot{q} = \dot{q}_{des}$, is then obtained using a first-order inversion of Eq. (4b).

The implementation commences with the α inversion to find $\dot{q}_{des}$.

1) Current values of α, q, δ_e, and V are used in conjunction with the tabular data to obtain $C_{Z_{total}}$. Substituting into Eqs. (6b) and (4a) yields the current estimate of $\dot{\alpha}$.

2) The current value of α is perturbed ± 1 deg, and new values of $\dot{\alpha}$ are found to establish $\partial\dot{\alpha}/\partial\alpha$. Then, q is perturbed to find $\partial\dot{\alpha}/\partial q$, which is usually close to unity.

3) The required $\dot{q}_{des}$ is found using Eq. (15) together with the derivatives obtained from step 2. The $\dot{\alpha}$ used in the right-hand side of Eq. (15) is the value computed in step 1 rather than an actual measurement.

Having found $\dot{q}_{des}$, the q inversion solves for δ_e using a recursive algorithm. This is necessary because the pitch moment data from Ref. 19 are not affine in δ_e and a closed-form solution for δ_e is not possible. Thus, δ_e is computed as follows.

4) Current values of α, q, V, and δ_e are used in conjunction with the tabular data to obtain $C_{m_{total}}$. Then the current estimate of $\dot{q}$ is obtained using Eqs. (4b) and (6c).

5) The current value of δ_e is perturbed ± 1 deg and substituted into Eq. (4b) to give new values of $\dot{q}_{des}$ and establish the value of $\partial\dot{q}/\partial\delta_e$.

6) Newton's method is used to estimate δ_e required to produce $\dot{q} = \dot{q}_{des}$.

7) Current values of α, q, V, and the latest iteration of δ_e from step 6 are used in conjunction with the tabular data to obtain $C_{m_{total}}$ and a new estimate of $\dot{q}$ is obtained using Eq. (4b).

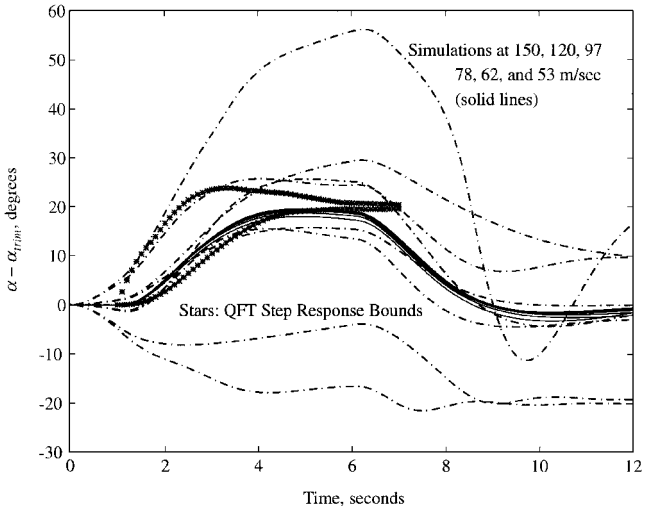

Fig. 9 Dynamic inversion α responses $1/(s^2 + 1.4s + 1)$ without QFT.

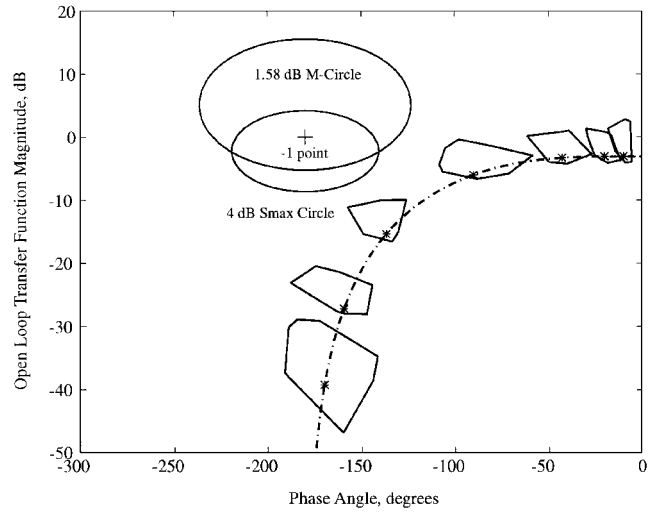

Fig. 10 Dynamic inverson uncertainty templates, $1/(s^2 + 1.4s + 1)$.

8) If $|\dot{q} - \dot{q}_{\text{des}}| < 0.001$ rad/s^2, the latest iteration on δ_e is considered an adequate solution and the iteration loop is exited. Otherwise, the procedure returns to step 5.

The iterative nature of this algorithm causes simulation times to increase by a factor of 4–6 compared with the linear controller described in Sec. VI.

Figure 9 shows responses of the aircraft to the test maneuver with the dynamic inversion implemented on its own without the QFT outer loops. Notice that the nominal responses (solid line) are good and fall well within the specifications of Sec. V. However, the perturbed responses at 150 m/s are extremely scattered, completely unsatisfactory, and border on instability. The raw dynamic inversion described is not robust to model perturbations.

C. LTIE Models and Templates

In contrast to the high-gain controller used to extract input/output signals in Sec. VI.A, here a high-gain dynamic inversion is used. The algorithm of Sec. VII.B is used with ν given by

$$\nu = 100\alpha_{\text{filt}} - 99\alpha - 12.6\dot{\alpha}_{\text{est}} \tag{16}$$

The term $\dot{\alpha}_{\text{est}}$ is an estimate of $\dot{\alpha}$ computed within the dynamic inversion algorithm. Combining Eqs. (13) and (16) yields dynamics between α_{filt} and α as

$$\frac{\alpha(s)}{\alpha_{\text{filt}}(s)} = \frac{100}{s^2 + 14s + 100} \tag{17}$$

This scheme worked well at all flight speeds and with perturbations to the pitching moment data. Over 40 high-gain simulations were conducted with the dynamic inversion inner loops closed using nominal aerodynamic data at speeds from 53 to 150 m/s and with α steps ranging from -18 deg below trim to 32 deg above. After completing this simulation series, an additional 40 simulations were run, eight at each of the five flight conditions, which had formed template extremities with the nominal data. These simulations were conducted with the three derivatives C_{m_α}, $C_{m_{\delta_e}}$, and C_{m_q} perturbed $\pm 20\%$ in all possible combinations to determine the sensitivity of the dynamic inversion control law to differences between the computational model used in the control law algorithm and the actual aircraft dynamic equations.

LTIE models were extracted from each of these high-gain simulations using GOLUBEV. Transfer functions were fitted between the ν signal and α. The transfer function between these two signals is nominally $P_{\text{DI}}(s) = 1/(s^2 + 1.4s + 1)$. The resulting templates (Fig. 10) are much smaller than the baseline templates in Fig. 6, which demonstrates the effectiveness of the dynamic inversion in transforming the nonlinear dynamics to linear time invariant.

D. QFT Design with Dynamic Inversion

The design of a QFT controller for the α loop shown in Fig. 8 follows the same procedure as the baseline design except that the

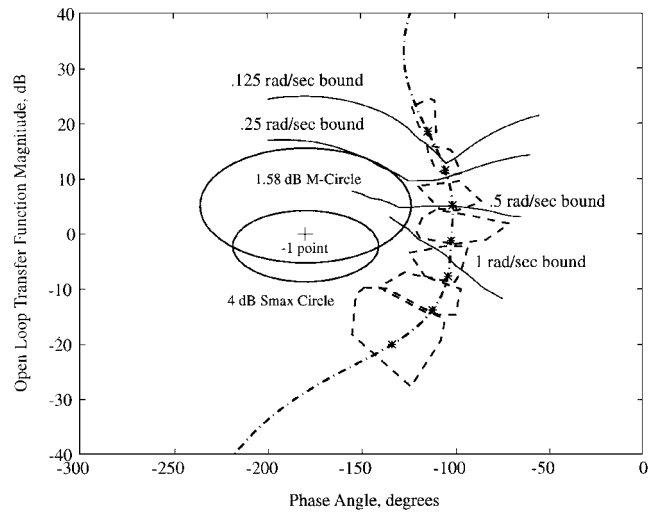

Fig. 11 Compensated templates for $1/(s^2 + 1.4 + 1)$ dynamic inversion.

new templates of Fig. 10 are used in place of the templates from Fig. 6. The effect of compensation on the templates is shown in Fig. 11, where $G(s)$ is

$$G_{\text{QFT}}(s) = \frac{300(s + 0.08)[s^2 + 1.4(1.05)s + 1.05^2]}{s(s + 0.02)[s^2 + 1.4(16)s + 16^2]} \tag{18}$$

The small template sizes allow a crossover of about 1 rad/s without violating any design boundaries. The prefilter $F(s)$ used with this design has a bandwidth of about 3 rad/s because the system already has a bandwidth of only about 1 rad/s:

$$F_{\text{QFT}}(s) = \frac{9}{(s^2 + 4.2s + 9)} \tag{19}$$

A second design for $G(s)$ having higher gain was made with this modified dynamic inversion structure. Its transfer function is given by

$$G_{\text{QFT}}(s) = \frac{1600(s + 0.12)[s^2 + 1.4(1.05)s + 1.05^2]}{s(s + 0.02)[s^2 + 1.4(24)s + 24^2]} \tag{20}$$

This produces a crossover about 2 rad/s and yields improved performance in the presence of plant perturbations. The baseline prefilter given by Eq. (9) is used with this design.

Finally, as an exercise, dynamic inversion was applied with $P_{\text{DI}}(s) = 1/s^2$. This yielded the templates shown in Fig. 12. The handle transfer function is $P_{\text{DI}}(s) = 1/s^2$, denoted by an asterisk in each template. The nominal templates (solid line) are much smaller than the baseline templates in Fig. 6. However, when the 20% perturbations are included, the templates (dashed line) grow drastically

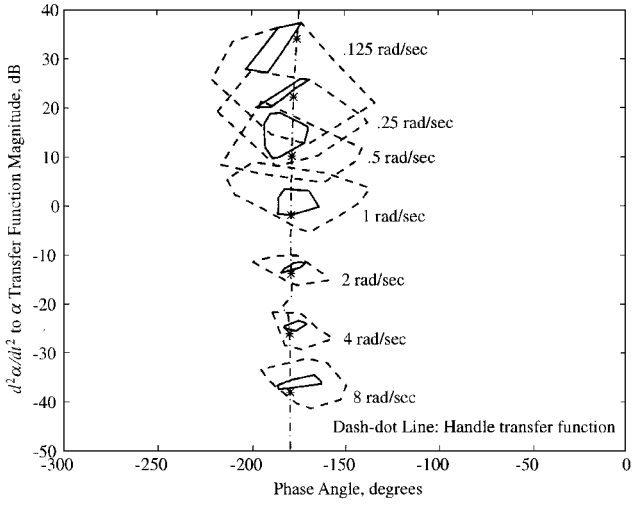

Fig. 12 Uncertainty templates with $1/s^2$ dynamic inversion.

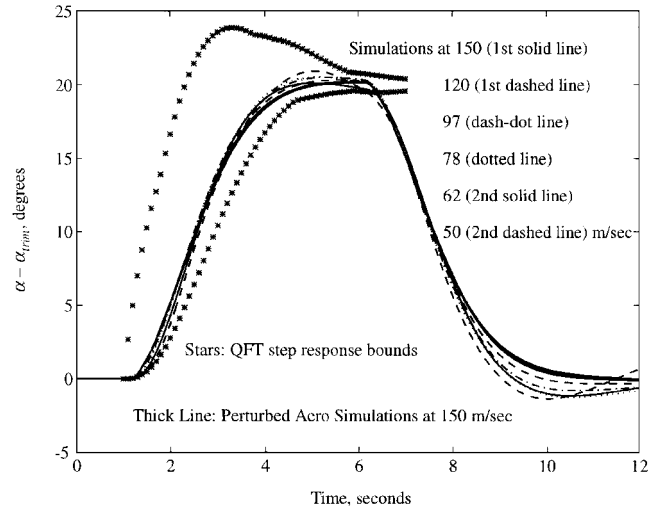

Fig. 13 Baseline QFT control law α responses.

bigger especially at low frequency. This is exactly what was predicted in Sec. VII.A and is proof that $P_{\mathrm{DI}}(s) = 1/s^2$ is a bad choice. The loop compensator with $P_{\mathrm{DI}}(s) = 1/s^2$ is

$$G_{\mathrm{QFT}}(s) = \frac{1900[s^2 + 1.9(0.18)s + 0.18^2](s + 0.18)}{s^2[s^2 + 1.4(24)s + 24^2]} \qquad (21)$$

The main problem here is that high gain is needed to meet the tracking boundary requirements in the presence of the large magnitude and phase variations at low frequency. This leads to a crossover between 4 and 8 rad/s, which is even higher than the fixed-gain baseline QFT design. Furthermore, any plant having the form $1/s^2$ requires additional phase lead near crossover, which is inconvenient. Notice also that, despite the fact that $P_{\mathrm{DI}}(s)$ is nominally a double integrator, $G_{\mathrm{QFT}}(s)$ still requires integrators to produce zero steady-state errors.

VIII. Simulations

Figures 13–16 show the results of simulating a 20-deg square pulse in α_{stick} of 5-s duration, commencing at time $t = 1$ s using the controller designs just described at various flight conditions with both nominal and perturbed aerodynamic data. The nominal simulations were conducted at speeds of 53, 62, 78, 97, 120, and 150 m/s. Only the results of perturbing the three derivatives, C_{m_α}, $C_{m_{\delta_e}}$, and C_{m_q}, at 150 m/s are shown because it was found that perturbations in the aerodynamic data have a more pronounced effect at 150 m/s than at lower speeds. This was especially true with the dynamic inversion designs because they use control inputs to cancel nominal terms in the dynamic equations. The aerodynamic terms, which are proportional to V^2, are much bigger at higher speed, leading to larger discrepancies between nominal and actual data.

Figure 13 shows the α response with the baseline QFT control law. The solid curves denote the responses with nominal data, whereas the dashed curves represent the 150-m/s perturbed data responses. All of the responses remain tightly clustered and fall between the two bounding curves adapted from Fig. 3.

The hybrid dynamic inversion with a bandwidth about 1 rad/s has very precise nominal responses (solid line, Fig. 14). The perturbed responses (dashed line) are more scattered than the baseline but remain close to the bounding responses and are considered acceptable. Figure 15 shows the responses for the modified dynamic inversion with the 2-rad/s crossover. As expected, the perturbed responses are clustered more tightly than those in Fig. 14, showing a correlation between tracking precision and increased loop gain. The benefit of using the QFT outer loops is seen by comparing these responses to the raw dynamic inversion responses in Fig. 9.

Figure 16 shows a comparison of the elevator response of the three controllers with nominal data at 150 m/s. Here the benefit of having dynamic inversion is evident by the gentler demands on elevator deflection. This contrasts with the oscillatory excursions produced by the baseline control law. Elevator oscillations with the baseline QFT

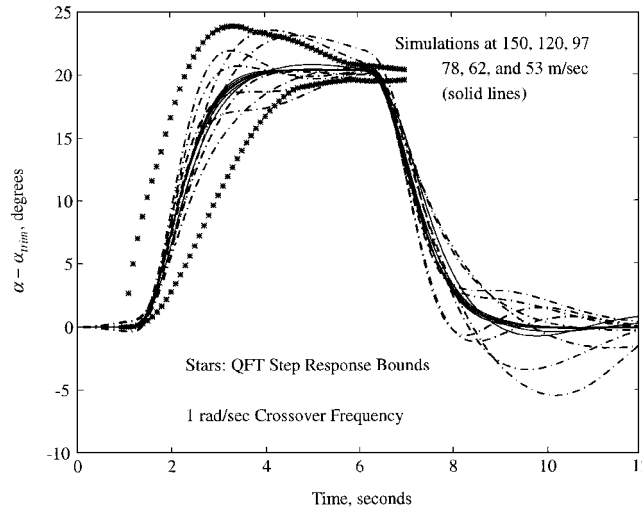

Fig. 14 Hybrid dynamic inversion and 1-rad/s bandwidth α responses.

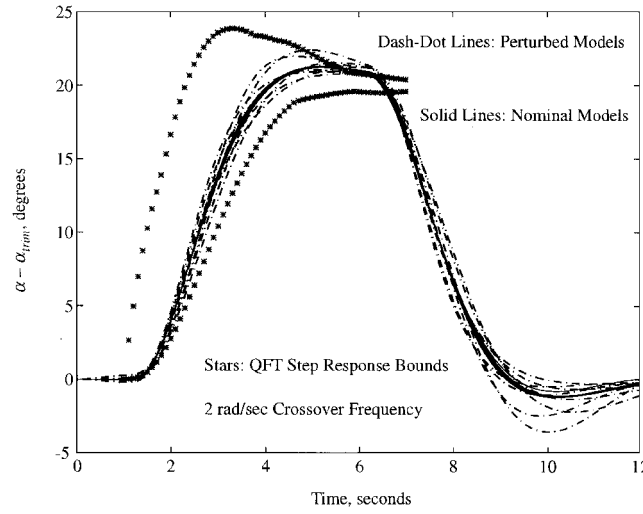

Fig. 15 Hybrid dynamic inversion and 2-rad/s bandwidth α responses.

were encountered at high speeds in Ref. 10. The oscillations result from the high gain in the baseline compensator $G(s)$, which is necessary to meet tight specifications on the closed-loop α-response over a wide speed range. The high gains provide performance robustness, but the loop gains become excessive at high speeds where control effectiveness is also much greater. The hybrid dynamic inversion-based control laws adjust for plant variation due to known nonlinearity so that the controller gain is reduced at higher speeds.

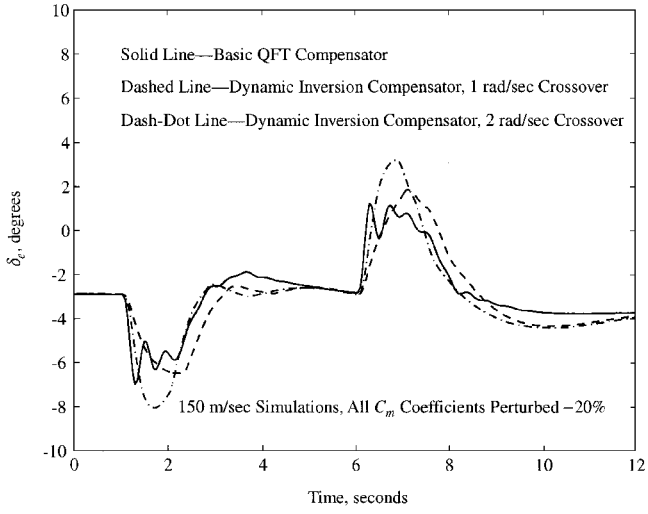

Fig. 16 Elevator deflections for baseline and hybrid dynamic inversion control.

IX. Conclusions

Conventional QFT provides a means to design linear control laws that are robust to wide variations in flight conditions. This paper demonstrates a successful use of the technique in the baseline design. A single linear compensator was designed for the F-16 short-period model that accurately controls α over a range of flight speeds corresponding to a 9:1 variation in dynamic pressure and $\pm 20\%$ variations in the pitching moment derivatives. The 20-deg pull-up maneuvers were well controlled at all speeds, but at the highest speeds the elevator oscillates severely, causing small ripples in the pitch rate trace, which are almost undetectable in the AOA history.

The results from the hybrid $1/(s^2 + 1.4s + 1)$ dynamic inversion are very promising. The nonlinear aircraft dynamics map to small templates on the Nichols chart, permitting very low crossover frequencies to be used. The time histories resulting from this low-gain (1-rad/s) dynamic inversion were prone to more variation due to plant perturbations but remained acceptable in terms of the design specifications. The lower gains permitted by the dynamic inversion lead to less aggressive demands on elevator displacements and rates compared to the high-bandwidth baseline design. The higher-gain (2-rad/s) dynamic inversion design produced tighter tracking, showing that the designer can readily alter the design to achieve higher performance vs lower bandwidth. It was also shown that the choice of desired dynamics $P_{\mathrm{DI}}(s)$ can be critical to the success of the dynamic inversion. The effect of an ill-considered choice for $P_{\mathrm{DI}}(s)$ was demonstrated in the case of $P_{\mathrm{DI}}(s) = 1/s^2$, which yields enormous low-frequency templates and requires high bandwidth to recover the performance robustness. It was recommended that $P_{\mathrm{DI}}(s)$ have stable poles with approximately the same magnitude as the open-loop aircraft. This would require close to minimal control energy from the dynamic inversion. Future work will apply these ideas to MIMO systems.

References

[1]Francis, M. S., "X-31—An International Success Story," *Aerospace America*, Feb. 1995, pp. 22–32.

[2]Reigelsperger, W. C., "Application of Multivariable Control Theory to Aircraft Control Laws," U.S. Air Force Wright Labs., TR WL-TR-96-3099, Wright–Patterson AFB, OH, May 1996.

[3]Horowitz, I. M., *Synthesis of Feedback Systems*, Academic, New York, 1963.

[4]Horowitz, I. M., *Quantitative Feedback Design Theory (QFT)*, Vol. 1, QFT Publications, Boulder, CO, 1993.

[5]D'Azzo, J. J., and Houpis, C. H., *Linear Control System Analysis and Design*, 4th ed., McGraw–Hill, New York, 1995, Chap. 18.

[6]Houpis, C. H., Sating, R. R., Rasmussen, S., and Sheldon, S., "Quantitative Feedback Theory Technique and Applications," *International Journal of Control*, Vol. 59, No. 1, 1994, pp. 39–70.

[7]Hess, R. A., and Gorder, P. J., "Quantitative Feedback Theory Applied to the Design of a Rotorcraft Flight Control System," *Journal of Guidance, Control, and Dynamics*, Vol. 18, No. 4, 1993, pp. 748–753.

[8]Reynolds, O. R., Pachter, M., and Houpis, C. H., "Full Envelope Flight Control System Design Using Qualitative Feedback Theory," *Journal of Guidance, Control, and Dynamics*, Vol. 19, No. 1, 1996, pp. 23–29.

[9]Horowitz, I., "Improvement in Quantitative Nonlinear Feedback Design by Cancellation," *International Journal of Control*, Vol. 34, No. 3, 1981, pp. 547–560.

[10]Snell, S. A., and Stout, P. W., "Quantitative Feedback Theory with a Scheduled Gain for Full Envelope Longitudinal Control," *Journal of Guidance, Control, and Dynamics*, Vol. 19, No. 5, 1996, pp. 1095–1101.

[11]Shamma, J. S., and Athans, M., "Gain-Scheduling: Potential Hazards and Possible Remedies," *IEEE Control Systems Magazine*, Vol. 12, No. 3, 1992, pp. 101–107.

[12]Snell, S. A., Enns, D. F., and Garrard, W. L., "Nonlinear Inversion Flight Control for a Supermaneuverable Aircraft," *Journal of Guidance, Control, and Dynamics*, Vol. 15, No. 4, 1992, pp. 976–984.

[13]Bugajski, D. J., and Enns, D. F., "Nonlinear Control Law with Application to High Angle-of-Attack Flight," *Journal of Guidance, Control, and Dynamics*, Vol. 15, No. 3, 1992, pp. 761–767.

[14]Enns, D., Bugajski, D., Hendrick, R., and Stein, G., "Dynamic Inversion: An Evolving Methodology for Flight Control Design," *International Journal of Control*, Vol. 59, No. 1, 1994, pp. 71–91.

[15]Buffington, J. M., Adams, R. J., and Banda, S. S., "Robust, Nonlinear, High Angle-of-Attack Control Design for a Supermaneuverable Vehicle," AIAA Paper 93-3774, Aug. 1993.

[16]Reiner, J., Balas, G. J., and Garrard, W. L., "Robust Dynamic Inversion for Control of Highly Maneuverable Aircraft," *Journal of Guidance, Control, and Dynamics*, Vol. 18, No. 1, 1995, pp. 18–24.

[17]Snell, S. A., and Stout, P. W., "Full Envelope Longitudinal Control Law Using a Nonlinear Controller Combined with QFT," *Proceedings of the Dynamic Systems and Control Division*, ASME DSC-Vol. 57-1, American Society of Mechanical Engineers, San Francisco, 1995, pp. 265–274.

[18]Golubev, B., and Horowitz, I. M., "Plant Rational Transfer Function Approximation from Input-Output Data," *International Journal of Control*, Vol. 36, 1982, pp. 711–723.

[19]Nguyen, L. T., Ogburn, M. E., Gilbert, W. P., Kibler, K. S., Brown, P. W., and Deal, P. L., "Simulator Study of Stall/Post Stall Characteristics of a Fighter Airplane with Relaxed Longitudinal Static Stability," NASA TP 1538, Dec. 1979.